Journal of Additive Manufacturing Technologies
DOI: 10.18416/JAMTECH.2111592

Infinite Science | Publishing

Comparison of Finite Element and Empirical Model Prediction of Surface Residual Stress in Inconel 718 Parts Fabricated by Laser Powder Bed Fusion Additive Manufacturing

M. Kaya[1*], N. Sunay[1], Y. Kaynak[2], F. Pıtır[3]

[1] *Department of Mechanical Engineering, Institute of Pure and Applied Sciences, Marmara University, 34722 Istanbul, Turkey*
[2] *Department of Mechanical Engineering, Technology Faculty, Marmara University, 34722 Istanbul, Turkey*
[3] *Ermaksan, Additive Manufacturing, 16065, Nilüfer, Bursa, Turkey*

[*] *Corresponding author, email: mertkaya6@marun.edu.tr*

Abstract

Inconel 718 parts produced by Laser Powder Bed Fusion (LPBF) generally have excessive residual stresses (RS) due to the extreme temperature gradients and high cooling rates that occur during production. These stresses can damage the mechanical properties and fatigue life of parts. Therefore, residual stress is one of the main reasons that hinder the widespread use of the LPBF process. The main purpose of this study is to predict the residual stress using finite element modeling and empirical approach of the production process in order to minimize the residual stress and distortions that occur during production. According to the simulation and theoretical calculation results, it has been observed that the residual stress in the build direction are generally large tensile stresses in the upper and lower regions and compressive stresses in a large middle region in between. One of the most important parameters that determine the residual stress magnitude is the scanning speed, which affects the energy density. The change in energy density due to constant laser power and increasing laser speed alters the amount of residual stress in the parts. This paper illustrates that when fabricating components with lower energy density leads to an increase of tensile residual stress, however, increasing energy density with altering process parameters results in reduced tensile residual stress.

Keywords: Laser powder bed fusion, Finite element modeling, Residual stress

1. Introduction

Additive manufacturing (AM) is an emerging approach considered as an alternative to traditional manufacturing methods. The main advantages of these manufacturing approaches are being able to produce parts with very complex geometry, reducing the number of processes to fabricate complex parts, etc. Although, a number of AM approaches are available, laser powder bed fusion (LPBF) is one of the commonly used in industries and also academia to fabricate metal components including Ni and Ti based alloys[1-3]. Inconel 718 alloy as one of the commonly used Ni based alloy, used in the aerospace industry, thanks to its superior properties such as maintaining its mechanical properties at high temperatures, high tensile, breaking and breaking strength [4]. Therefore, its production with LPBF technology is very important.

Due to repeated rapid thermal heating and cooling cycles during the LPBF process, high residual stresses occur in its parts [5]. Residual stress significantly affects the dimensional accuracy and mechanical performance of the formed parts [6]. The methods used for the determination of residual stress values such as X-Ray [7], three-prong method [8]and neutron diffraction [9] are quite costly and complex. With the model developed by Carlsson et al. [10, 11] using the experimental link between microhardness measurement parameters and residual stresses, it is possible to quickly predict residual stress values.

In the literature, there are many studies examining the residual stresses occurred within the parts produced by the LPBF method. Prabhat Pant et al. [12] investigated the effect of structure orientation on residual stress distribution and observed that little stress occurs on parts printed in the horizontal direction. Xu Song et al. [13] aimed to optimize the production parameters by performing finite element modeling of the manufacturing process in order to minimize residual stresses and distortions. Xiaoqing Wang et al. [5] presented that stress relieving heat treatment provides an increase in hardness of parts and has a significant effect on the reduction of residual stresses. Naresh Nadammal et al. [14] confirmed that the residual stresses generated during powder bed fusion additive manufacturing can be controlled by changing the

scanning strategies. However, extensive study is still needed to further understand the effect of variations of thermal gradients and cooling rates caused by the laser parameters used in the LPBF process on the residual stress.

In this study, Inconel 718 samples are produced by using LPBF at constant laser power and various scanning speeds. By utilizing empirical approaches, RS resulting from additive manufacturing is calculated. Besides, FEM approach through Simufact Additive is utilize to simulate AM process of this parts and resulting residual stresses are predicted. The comparison in between empirical model and FEM result are compared and presented in this work.

2. Material and methods

2.1. Powder material

Inert gas atomized pre-alloyed IN718 superalloy powders with a particle size of 15-45 µm were provided by "AP&C GE Additive". Table 1 shows the chemical composition of the powder.

Table 1. Chemical composition (wt.%) of IN718 powder [15].

Element	Ni	Cr	Fe	Nb	Mo
Weight %	53.32	18.99	18.01	5.01	3.04
Element	Ti	Al	Co	C	O
Weight %	0.91	0.46	0.06	0.05	0.022

2.2. Fabrication of samples and characterization

The samples were produced on the "ERMAKSAN EnaVision 3D Additive Manufacturing Machine" with the process parameters shown in Table 2 using the laser powder bed fusion method. This machine has a laser type with a maximum power of 500W and a spot diameter of 85 µm. 15x15x15 coupons were produced with the chessboard scanning strategy. Based on a series of preliminary experiments, the laser power (P) was kept constant at 280 W and scanning speeds (V) were varied as 400, 1000, 1600, 2200 mm/s. Process parameters is shown in Table 2.

Table 2. Parameters of the LPBF process.

Laser power P, (W)	**Laser scan speed *V*, (mm/s)**	**Energy Density (J/mm³)**
280	400	194.4
	1000	77.7
	1600	48.6
	2200	35.3

Constant Parameters
Hatch distance h, mm : 0.12
Layer thickness d, mm : 0.03
Laser focus diameter f_d, mm : 0.085
Recoater time s, sec : 11
Scan Strategy : Chessboard

The microhardness of all fabricated samples was measured to use residual stress calculation. A 3D Keyence VHX-6000 optical microscope was used to examine the topography of the parts. The ASTM E 384 standard was followed for the hardness test using Future-Tech FM310e. By taking 6 measurements from both the scanning and build directions, with a dwelling time of 15 seconds, the hardness of each specimen was determined and a test load of 100 gf was used. Figure 1 shows the geometry of the tip in the vickers hardness device and the geometry formed by the penetrating tip formed in the Inconel 718 workpiece after the hardness measurement.

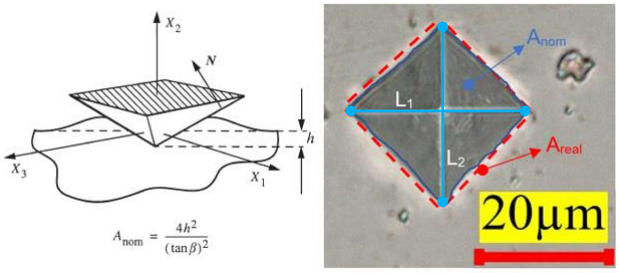

Fig 1. (a) Tip geometry in Vickers hardness device [10] and (b) Diagram of the nominal projected contact area A_{nom} and the actual contact area of the sample A_{real}.

2.3. Residual stress calculation

In this study, residual stress is not directly measured instead it is calculated by utilizing the empirical approaches developed by Carlsson and Larsoon [10, 11]. Their model has been utilized by many researchers to calculate residual stress resulting from AM processes [2, 16, 17].

The equations from 1 to 14 have been borrowed from [10, 11] and utilized to calculate residual stress.

Hardness is expressed by the formula given below [10, 11].

$$H = C\sigma_Y \quad (1)$$

Here, the C value is taken as a constant depending on the insert geometry used in the hardness measurement. σ_Y is the yield stress. In hardening materials, σ_{repr} is used instead of σ_Y, and it expresses the flow stress corresponding to the plastic unit deformation (ε_{repr}) [10, 11].

$$H = C\,\sigma_Y(\varepsilon_{repr}) \quad (2)$$

In order to accurately predict the hardness change due to residual plastic strain, the expression in Equation 2 can be written as follows [10, 11];

$$H = C\,\sigma_Y\,(\varepsilon_{repr} + \varepsilon_{res}) \quad (3)$$

The H value represents the microhardness of the place where the measurement is made and can be written as follows [10, 11].

$$H = \frac{P}{A} \quad (4)$$

Here, P is the load and A is the area, but in microhardness, it is expressed as follows and the A_{surf} is given as the area of the immersing tip [16].

$$HV = \frac{P}{A_{surf}} \quad (5)$$

A new parameter (c^2) has been added to their model to calculate the residual stress by creating a correlation between the coaxial residual stress/strain areas and the contact area/microhardness [10, 11],

$$c^2 = \frac{A_{real}}{A_{nom}} \quad (6)$$

where A_{real}, represents the actual contact area of a sample exhibiting sinking or stacking, A_{nom} is the nominal contact area calculated directly from the indentation depth (h_{max}) without considering sinking or stacking along the contact boundary [10, 11],

$$A_{nom} = \left(\frac{2h_{max}}{tan22^o}\right)^2 = 24.5h_{max}^2 \quad (7)$$

In the study of Carlsson et al., the residual stress is expressed as [10, 11],

$$c^2 = c_0^2 - 0.32 \ln\left(1 + \frac{\sigma_{res}}{\sigma(\varepsilon_{res})}\right) \quad (8)$$

Here; ε_{res} is the residual plastic deformation that can be deduced from the hardness change according to the Tabor equation. It is the flow stress when $\sigma(\varepsilon_{res})$ is equal to the plastic strain (ε_{res}). c^2 and c^2 c_0^2, are the area ratios for the case where both the residual stresses and the original material are present, respectively. L_1 and L_2 represent the trace lengths formed by the immersing tip [5, 16].

$$A_{nom} = \frac{1}{2}\left(\frac{(L_1+L_2)}{2}\right)^2 \quad (9)$$

The stress-strain curve obtained by Liu et al. was used in this study and the tensile test results were obtained with an approximate power function approximation [16, 18],

$$\sigma(\varepsilon_{res}) = \sigma_0\, \varepsilon_{res}^n = 1181.21\, \varepsilon_{res}^{0.1754} \quad (10)$$

So with the following formulas [16],

$$\varepsilon_{res} = \left(\frac{P}{C\sigma_0 * A_{nom}}\right)^{\frac{1}{n}} - \epsilon_{repr} \quad (11)$$

$$\sigma_{res} = \sigma(\varepsilon_{res}) * \left[e^{\left(\frac{c_0^2 - c^2}{0.32}\right)} - 1\right] \quad (12)$$

residual stresses can be calculated with the formula in Equation 13 [16].

$$\sigma_{res} = \sigma_0 \left\{\left[\frac{8*P}{C\sigma_0*(L_1+L_2)^2}\right]^{\frac{1}{n}} - \epsilon_{repr}\right\}^n * \left\{e^{\left[\frac{c_0^2 - \frac{8*A_{real}}{(L_1+L_2)^2}}{0.32}\right]} - 1\right\} \quad (13)$$

When using a Vickers tip, values , C=3, ε_{repr}=0.08 and c_0^2=1can be used [11, 16].

$$\sigma_{res} = 1181.21 \left\{\left[\frac{8*P}{3*1181.21*(L_1+L_2)^2}\right]^{\frac{1}{0.1754}} 0.08\right\}^{0.1754} * \left\{e^{\left[\frac{1 - \frac{8*A_{real}}{(L_1+L_2)^2}}{0.32}\right]} - 1\right\} \quad (14)$$

As a result, residual stresses can be determined by the formula presented above.

Vickers notch tests were measured close to the untreated surface, creating 6 notches for each sample in the scan direction and the build direction. The force applied for the tests in the Vickers microhardness measuring device is 100 gf, and also L_1 and L_2 values were recorded during the indentation process. Afterwards, the areas (A_{real}) of the formed indentations were measured under a digital microscope, and the L_1 and L_2 values recorded during the indentation were confirmed under the digital microscope, and it was aimed to minimize the error rate by performing a more precise measurement as a decimal. By replacing the obtained measurements in the formula in Equation 14, 6 different residual stress values were obtained for each sample and the arithmetic average of the obtained values was taken and the standard deviation was calculated.

2.4. Finite Element Model

Simufact Additive 2021 software was used in the simulation phase of the production process of Inconel 718 by LPBF. This software is used to simulate metal additive manufacturing production processes and to analyze the effects of production parameters (distortion, residual stress, strain, etc.) on the part resulting from production.

Fine mesh hexahedral elements of 0.05 mm x 0.1 mm x 0.05 mm were adopted for the parts. Baseplate dimensions are 100x100x7 mm by default. In addition, comparatively coarse hexahedral adaptive mesh was used for the base plate. In the simulation, the laser processing parameters were applied exactly, and the residual stresses on the parts as a result of the simulation were determined by taking six points from both the scanning and build directions as in the microhardness test performed in experimental methods.

3. Results and discussion

Figure 2 shows microhardness variation at build and scanning direction of samples as a function of laser scanning speed. Obvious trend at both build and scan direction can be observed. Increasing laser scanning speed results in reduced microhardness until 1600 mm/s then saturates as a function of laser scan speed at both direction of the sample.

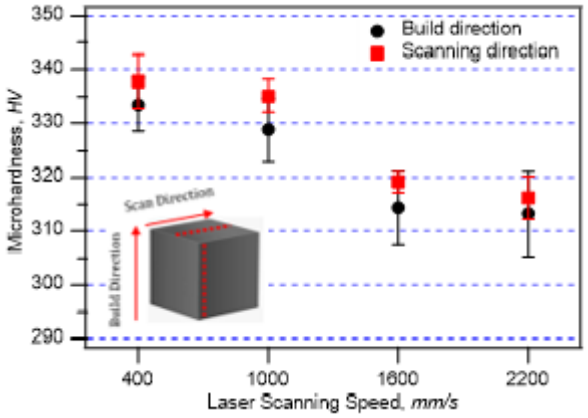

Fig 2. Effect of scanning speed on microhardness of different directions of samples.

Figure 3 shows the effect of laser scanning speed on residual stress of building direction of the sample. It includes both empirical calculation and simulation results. From simulation, it is apparent that the there is a large variation in between the surface and core of the specimens in terms of residual stress. While, the core of sample has large compressive residual stress, the surface of the sample has tensile residual stress. This is the typical response when we consider build direction in SEM simulation. Considering calculation made based on empirical model presented in Figure 3, it confirms that tensile residual stress at the surface of the specimen takes place. However, it should be noted that empirical calculation does not consider the core of the specimen as the microhardness is measured from the surface of the produced specimen. Figure 3 also shows an important point is that while energy density (approximately 194.4 J/mm^3) is high enough at 400 mm/s laser scanning speed, no crack is observed on the produced sample; however, when energy density becomes low (approximately 35.3 J/mm^3) at high laser scanning speed, 2200 mm/s, the crack is observed. On the other hand, the predicted overall trend through numerical simulation and empirical calculation is that as scanning speed increases, the trend of residual stress is increased. Both empirical calculation and numerical predictions have same trend. For instance, while predicted tensile residual stress is about 428 MPa when laser scanning speed is 400 mm/s, it becomes almost 440 MPa when scanning speed becomes 2200 mm/s. Indeed, the variation is too small but overall trend shows increasing trend. Empirical calculation based on hardness measurements from the fabricated samples also shows similar raising trend with increased scanning speed.

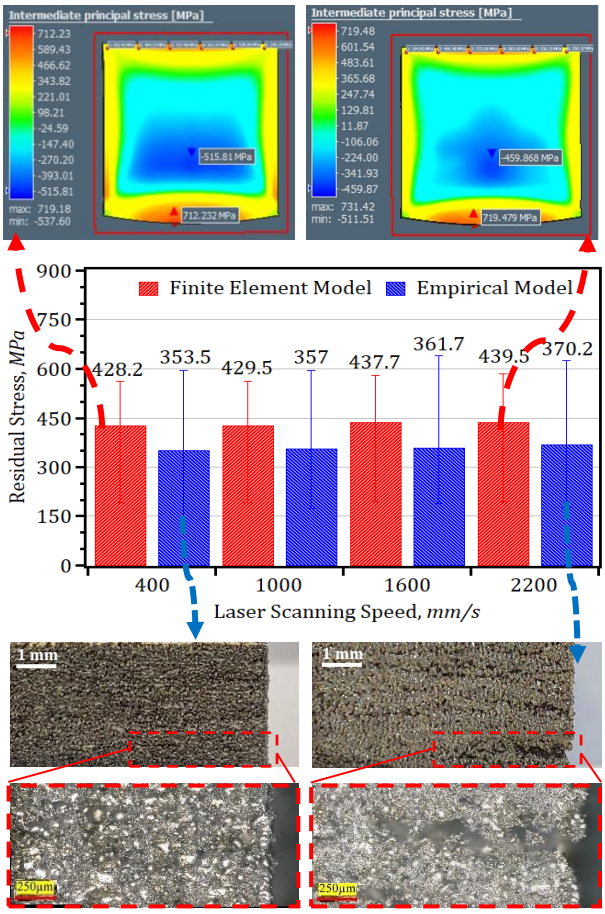

Fig 3. Residual stress values in the build direction determined by finite elements and theoretical calculation methods.

More or less similar trend is also observed when residual stress of scanning direction of samples is examined as shown in Figure 4. During the laser melting process, the thermal stress produced by the high temperature exceeds the yielding limit of the material, forming a melt pool, and residual stresses occur during cooling. Residual stress generation begin with thermal stress with an increase/decrease in temperature of several hundred Kelvin during manufacture, and the residual stress magnitude increase with further heating/cooling [19]. In addition, it can cause residual stresses due to the different coefficients of thermal expansion of different metals in the alloy [20]. While compressive residual stresses occur in the inner parts of the part, tensile residual stresses occur in the outer surfaces of the part. During the production process with LPBF, when the parts are built layer by layer, when the next melting layer re-melts or reheats the substrates, due to the temperature difference between the inner part of the part and the outer part, a residual compressive stress occurs in the interior, while tensile residual stress occurs in the outer part [21]. This is clearly seen in the simulation images in Figure 3. Since the material in the molten pool is constrained by the surrounding area during laser remelting, the temperature gradients and distribution in the unmelted area at the boundary of the molten pool determine the magnitude and effect of the residual stress generated [22].

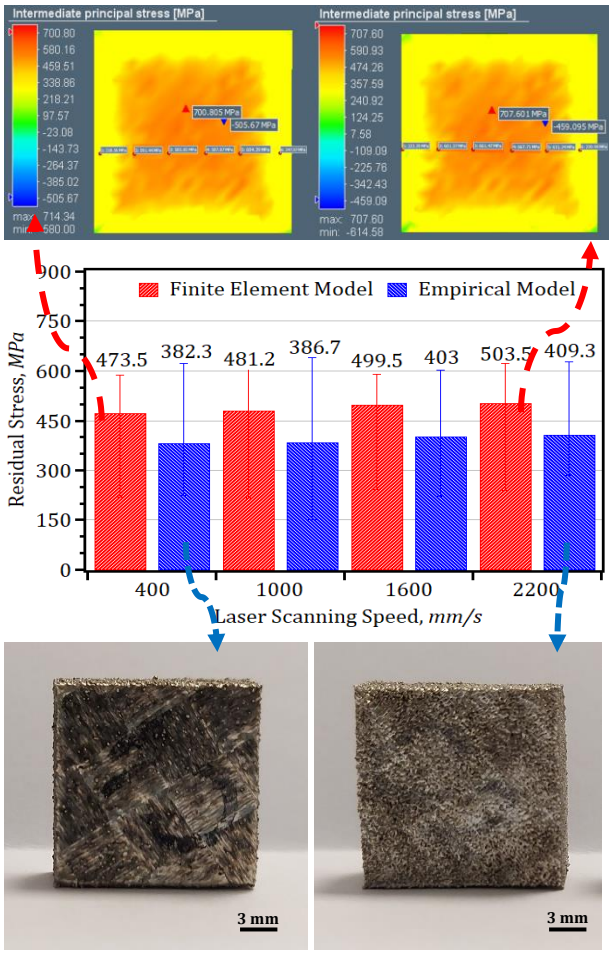

Fig 4. Residual stress values in the scan direction determined by finite elements and theoretical calculation methods.

In the tests performed, it is seen that the tensile residual stress values on the surface of sample increase as the laser scanning speed increases according to the results of both models. As the laser scanning speed increases, the irradiation time of the laser decreases, resulting in an increase in temperature gradients at the boundaries of the melt pool due to the uneven temperature distribution. This increase causes the magnitude of the tensile residual stress values to increase [23]. This increase in tensile residual stress leads to the formation of a crack in the build direction of the part as shown in Figure 3. It is also evident that the increase in laser scanning speed decreases the microhardness values in the build and scanning direction. This is thought to be due to the increase in the tensile residual stress values formed on the surface.

The residual stresses analyzed by both models have a large standard deviation, as also mentioned by Liu et al. [18] and Cao et al. [24]. The real residual stress values change from point to point due to the inhomogeneity of the microstructure properties of the produced parts is the main reason of such variation. In addition, Sebastiani et al. [25] reported that the residual stress values calculated in their study had a large standard deviation of 0.85 GPa. In addition, one of the reasons for the large standard deviation of the residual stresses analyzed with the empirical approach is that there are some errors brought by manual measurement in the measurement of A_{real} , L_1 and L_2 values.

4. Conclusions

Residual stress analyzes of Inconel 718 parts produced with LPBF were carried out using the finite element model and empirical model. The results obtained based on the experimental and simulation conclusions can be listed as follows.

(1) Residual stresses were unevenly distributed in the parts and there was no appreciable difference in both microhardness and residual stresses in the build direction and scan direction of the L-PBF Inconel 718 samples.

(2) Both approaches confirm that High laser scanning speed increased the tensile residual stress values on the part surface. This is the reason of observed cracks in the fabricated parts and also reduction of hardness on the surface.

(3) The residual stress results predicted by the empirical model were on average approximately 22% lower than the finite element model results. Considering the standard deviations of both models, it is possible to say that the results agree with each other.

Author's statement

Conflict of interest: Authors state no conflict of interest. Informed consent: Informed consent has been obtained from all individuals included in this study. Ethical approval: The research related to human use complies with all the relevant national regulations, institutional policies and was performed in accordance with the tenets of the Helsinki Declaration, and has been approved by the authors' institutional review board or equivalent committee.

References

1. Qian, Z., Chumbley, S., and Johnson, E., *The effect of specimen dimension on residual stress relaxation of carburized and quenched steels.* Materials Science and Engineering: A, 2011. **529**: p. 246-252.
2. Lu, Y., et al., *Study on the microstructure, mechanical property and residual stress of SLM Inconel-718 alloy manufactured by differing island scanning strategy.* Optics & Laser Technology, 2015. **75**: p. 197-206.
3. Gong, H., et al., *Influence of defects on mechanical properties of Ti–6Al–4 V components produced by selective laser melting and electron beam melting.* Materials & Design, 2015. **86**: p. 545-554.
4. Wang, X., Gong, X., and Chou, K., *Review on powder-bed laser additive manufacturing of Inconel 718 parts.* Proceedings of the Institution of Mechanical Engineers, Part B: Journal of Engineering Manufacture, 2017. **231**(11): p. 1890-1903.
5. Wang, X. and Chou, K., *The effects of stress relieving heat treatment on the microstructure and residual stress of Inconel 718 fabricated by laser metal powder bed fusion additive manufacturing process.* Journal of Manufacturing Processes, 2019. **48**: p. 154-163.
6. Wang, Z., et al., *Diffraction and single-crystal elastic constants of Inconel 625 at room and elevated temperatures determined by neutron diffraction.* Materials Science and Engineering: A, 2016. **674**: p. 406-412.
7. Song, X., et al., *Residual stresses and microstructure in powder bed direct laser deposition (PB DLD) samples.*

International Journal of Material Forming, 2015. **8**(2): p. 245-254.
8. Sillars, S., et al., *The three-prong method: a novel assessment of residual stress in laser powder bed fusion.* Virtual and Physical Prototyping, 2018. **13**(1): p. 20-25.
9. Wu, A.S., et al., *An experimental investigation into additive manufacturing-induced residual stresses in 316L stainless steel.* Metallurgical and Materials Transactions A, 2014. **45**(13): p. 6260-6270.
10. Carlsson, S. and Larsson, P.-L., *On the determination of residual stress and strain fields by sharp indentation testing.: Part I: theoretical and numerical analysis.* Acta materialia, 2001. **49**(12): p. 2179-2191.
11. Carlsson, S. and Larsson, P.-L., *On the determination of residual stress and strain fields by sharp indentation testing.: Part II: experimental investigation.* Acta Materialia, 2001. **49**(12): p. 2193-2203.
12. Pant, P., et al., *Mapping of residual stresses in as-built Inconel 718 fabricated by laser powder bed fusion: A neutron diffraction study of build orientation influence on residual stresses.* Additive Manufacturing, 2020. **36**: p. 101501.
13. Song, X., et al., *Advances in additive manufacturing process simulation: Residual stresses and distortion predictions in complex metallic components.* Materials & Design, 2020. **193**: p. 108779.
14. Nadammal, N., et al., *Critical role of scan strategies on the development of microstructure, texture, and residual stresses during laser powder bed fusion additive manufacturing.* Additive Manufacturing, 2021. **38**: p. 101792.
15. Georgilas, K., Khan, R.H., and Kartal, M.E., *The influence of pulsed laser powder bed fusion process parameters on Inconel 718 material properties.* Materials Science and Engineering: A, 2020. **769**: p. 138527.
16. Wang, X. and Chou, Y.K. *A method to estimate residual stress in metal parts made by Selective Laser Melting*. in *ASME International Mechanical Engineering Congress and Exposition*. 2015. American Society of Mechanical Engineers.
17. Song, B., et al., *Vacuum heat treatment of iron parts produced by selective laser melting: microstructure, residual stress and tensile behavior.* Materials & Design (1980-2015), 2014. **54**: p. 727-733.
18. Liu, F., et al., *Microstructure and residual stress of laser rapid formed Inconel 718 nickel-base superalloy.* Optics & laser technology, 2011. **43**(1): p. 208-213.
19. DebRoy, T., et al., *Additive manufacturing of metallic components–process, structure and properties.* Progress in Materials Science, 2018. **92**: p. 112-224.
20. Bartlett, J.L. and Li, X., *An overview of residual stresses in metal powder bed fusion.* Additive Manufacturing, 2019. **27**: p. 131-149.
21. Ahmad, B., et al., *Residual stress evaluation in selective-laser-melting additively manufactured titanium (Ti-6Al-4V) and inconel 718 using the contour method and numerical simulation.* Additive Manufacturing, 2018. **22**: p. 571-582.
22. Jiang, X., Ye, T., and Zhu, Y., *Effect of process parameters on residual stress in selective laser melting of AlSi10Mg.* Materials Science and Technology, 2020. **36**(3): p. 342-352.
23. Sun, F.-Z., et al., *Effect of laser scanning speed on the thermal-mechanical coupling field of laser remelting of valve seat.* Optik, 2021. **225**: p. 165776.
24. Cao, J., et al., *Effect of overlap rate on recrystallization behaviors of Laser Solid Formed Inconel 718 superalloy.* Optics & Laser Technology, 2013. **45**: p. 228-235.
25. Sebastiani, M., et al., *Effects of residual stress on nano-mechanical behavior of thin films*, in *Nanomechanical Analysis of High Performance Materials*. 2014, Springer. p. 263-284.